ACS APPLIED MATERIALS & INTERFACES

Research Article

www.acsami.org

Hydrogel Nanomembranes as Templates for Patterned Deposition of Nanoparticles on Arbitrary Substrates

Nikolaus Meyerbröker[†] and Michael Zharnikov*

Applied Physical Chemistry, Heidelberg University, Im Neuenheimer Feld 253, 69120 Heidelberg, Germany

ABSTRACT: Patterns of nanoparticles (NPs) on solid supports are usually restricted to a particular substrate or a class of substrates. Here we present a procedure that decouples the patterning step from the target substrate, enabling the fabrication of custom designed NP assemblies on nearly any solid support, including nonflat ones. The procedure relies on a hydrogel template prepared on the primary, conductive substrate and transferred to the target support as a sacrificial nanomembrane. The template is structured by electron beam lithography (EBL) which seals predefined areas of poly-(ethylene glycol) based hydrogel film, making them inert to NP deposition in contrast to pristine areas that adsorb NPs in high densities. The deposition of NPs, occurring from an aqueous solution into the transferred membrane, follows EBL generated structure, delivering the desired NP pattern on the target support after removal of the organic matrix. Efficiency and flexibility of the procedure is illustrated by creating a variety of representative submicrometer patterns of densely packed gold and silver NPs on glass, including a useful pattern of a miniaturized quick-response code. The arrangement of NPs in these patterns corresponds to the negative image of EBL generated template. This significantly reduces the exposure time for designs where large areas covered with NPs are separated by thin, NP-free stripes.

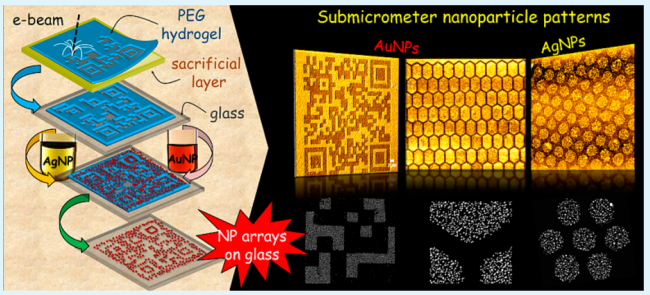

KEYWORDS: *nanoparticle patterns, gold nanoparticles, silver nanoparticles, electron beam lithography, poly(ethylene glycol), hydrogel membrane template, submicrometer QR-code*

1. INTRODUCTION

Inorganic nanoparticles (NPs) reveal a variety of unique properties, making them one of the primary objects in frontier research and, increasingly, in commercial products. These remarkable characteristics are related to the quantum-scale size and high surface to volume ratio.[1] Particularly, gold and silver NPs offer useful optical behavior in the visible range, relying on direct excitation of surface plasmon resonance (SPR) by light, which is impossible in the case of the respective bulk metals.[2−4] Because of the high extinction coefficient in the vicinity of SPR, optical detection even of individual NPs is possible.[5] Additionally, the position of the SPR band depends sensitively on dielectric properties of the surrounding medium. This makes localized SPR (LSPR) spectroscopy of metallic NPs a powerful technique for sensing experiments and allows fabrication of SPR-based chemical, physical and biological sensors.[6−8] Furthermore, LSPR is responsible for electromagnetic-field enhancement leading to surface-enhanced spectroscopic processes, with surface-enhanced Raman scattering (SERS) being the most prominent example.[9,10] It is also not irrelevant to mention that Au and Ag NPs are easy to synthesize and are stable in aqueous solutions as well as in a variety of organic solvents.[2] They are also easy to functionalize with suitable receptors serving, for instance, as medical diagnostic marker agents.[11]

A variety of NP applications such as particular biosensors or platforms for cell studies relies on their immobilization on solid supports. Depending on a particular goal, this immobilization can be performed either homogeneously[2,12,13] or as a pattern[14−32] which frequently needs to have a complex shape and/or custom design. In view of the above demands, a large variety of top-down based techniques has been developed, ranging from microcontact printing (μ-CP)[21] and nanoimprint lithography[22,23] for macroscopic, microscopic and submicrometer sized NP patterns to dip-pen lithography,[24] scanning probe lithography,[25] and colloidal lithography[20,21] for positioning individual NPs. Another prospective approach is electron beam lithography (EBL) representing a convenient method for fast micropatterning through a stencil mask or serial and flexible writing with a focused e-beam down to resolution of a few nanometers. Representative strategies within this general framework are e-beam assisted reduction of a gold ion precursor film[26−28] and ex situ deposition of preformed AuNPs from solution onto an appropriate structured substrate.[15,18,29,30] Note that the structuring can also be performed after NP deposition, by cross-linking the capping agent of deposited NPs.[20,31] The latter, ex situ methods offer the advantage of higher flexibility in respect to size, shape, and composition of the NPs because fabrication and immobilization steps are separated.

Received: July 4, 2014
Accepted: July 14, 2014
Published: July 14, 2014

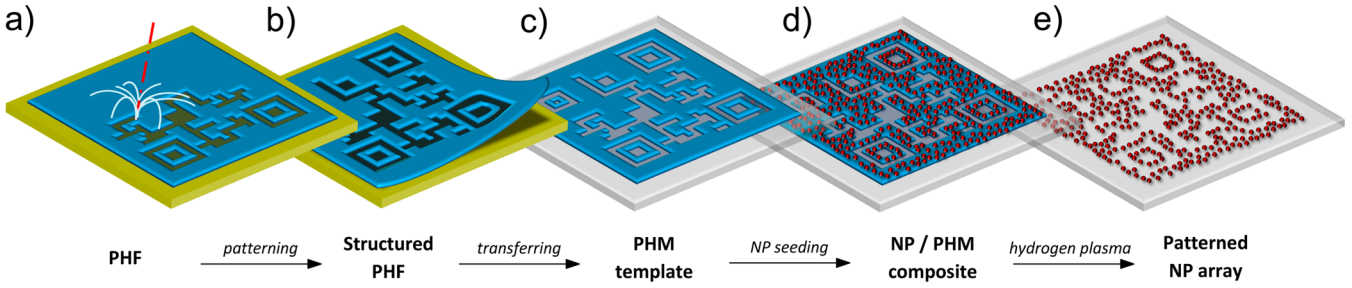

Figure 1. Schematic representation of the preparation process for tailor-made NP patterns on arbitrary substrates by means of a transient PEG hydrogel template: (a) PEG hydrogel film (PHF; blue) prepared on a primary, conductive substrate (yellow) is pattered by electron beam lithography; (b) structured PHF is released from the primary substrate and (c) transferred as a PEG hydrogel membrane (PHM) template onto a secondary substrate (gray); (d) directed deposition of NPs (red) into PHM template by immersion of the sample into an aqueous NP solution; (e) removal of PHM template by hydrogen plasma treatment releases the desired NP pattern on the secondary substrate.

Apart from advantages and inherent strengths, all above strategies for the fabrication of NP patterns rely on a selected substrate or a class of substrates, utilizing a specific chemistry or/and substrate properties. In particular, EBL-assisted pattern preparation can only be performed on a conductive and flat support, apart from restrictions related to specific chemistry used to control NP attachment.

In view of the above limitations, we present here a novel and universal route to prepare NP patterns. It is not linked to a specific substrate, but can be implemented for the fabrication of custom designed NP patterns on any solid support. The strategy relies on EBL, taking advantage of arbitrary shape of fabricated features as well as of sub-micrometer and nanometer resolution typical of this patterning technique. Also, it is not limited to noble metal (NPs) but can also be applied to semiconducting quantum dots (QD) or magnetic NPs, which are promising candidates in molecular electronics and magnetic storage devices.[17,33]

Key idea of the presented route is the use of an ultrathin hydrogel template transferred as a membrane from the primary substrate. Precursor of this membrane—a hydrogel film comprised of a highly cross-linked poly(ethylene glycol) (PEG)—is capable of adsorbing citrate-stabilized NPs in amazingly high densities.[34] When this film is irradiated by EBL, the exposed areas reduce significantly their ability to adsorb NPs.[35] Performing preparation and irradiation steps on a conductive sacrificial layer,[36] the PEG hydrogel film (PHF) can be transferred subsequently as a structured PEG hydrogel membrane (PHM) to a secondary, target substrate. The transferred template allows a controlled seeding of miscellaneous NPs by its immersion into their aqueous solution. After removal of the organic stencil, the desired NP arrangement is released on the target substrate as a perfect, negative copy of the e-beam pattern. This is especially of advantage for designs where large areas of NPs are separated by thin, particle-free stripes.

2. EXPERIMENTAL SECTION

PEG Hydrogel Films (PHF). Epoxy- and amine-terminated, 4-arm PEG precursors with 2 kDa (Creative PEGWorks, USA) were separately dissolved as 10 mg/mL solutions in chloroform. A 1:1 mixture of both precursor solutions was spin-coated onto a silicon substrate covered with 100 nm gold film (no adhesion layer between Si and Au) and thermally cross-linked under nitrogen atmosphere at 80 °C for 4 h. The thickness of the resulting PHFs was 60 nm with deviations of less than 5 nm

Structured PHF. The PHFs were patterned using a LEO 1530 Gemini scanning electron microscope (SEM) with a lithographic controller unit (Raith Elphy Quantum) as electron beam writer under high vacuum conditions. The electron energy was set to 3.0 keV and irradiation dose to 1 mC/cm^2.

PHM Template. Structured PHFs were spin-coated with a ∼100 nm layer of poly(methyl methacrylate) (PMMA) (950 kDa as 5% solution in chlorobenzene) to stabilize them during the transfer process. By careful immersion into water, the Au/PHF/PMMA sheet was detached from the silicon substrate. The sacrificial gold layer was dissolved by transferring the membrane on an aqueous gold etching solution containing I_2/KI. The remaining PHF/PMMA membrane was placed onto the target support (silicon or glass) providing the PHM template after eliminating PMMA with acetone.

NP Adsorption. Colloidal, citrate-stabilized AuNPs and AgNPs were prepared by reducing an aqueous solution of $HAuCl_4$ or $AgNO_3$ with sodium citrate, resulting in a purple or yellow suspension of the respective NPs.[37] NP seeding was performed by immersion of the substrate supported PHM template into NP solution for 18−24 h. Weakly bound NPs were removed by subsequent rinsing with water.

NP Patterns on Target Substrate. The hydrogel PEG template was removed by 45 min hydrogen plasma treatment (PVA TePla 100E, microwave plasma system, 0.4 mbar H_2 pressure at 150 W MW-power) releasing exclusively NPs on the substrate.

X-ray Photoelectron Spectroscopy. The X-ray photoelectron (XP) spectrometer (MAX200, Leybold-Heraeus) was equipped with an Mg Kα X-ray source (1253.6 eV; 200 W) and a hemispherical analyzer. The recorded spectra were normalized to the spectrometer transmission function. The spectrometer work function was referenced to the Au $4f_{7/2}$ emission of clean gold at 84.0 eV. The spectra were fitted by symmetric Voigt functions and a Shirley-type background within the evaluation procedure.

Scanning Electron Microscopy. SEM images of NP patterns were taken with a LEO 1530 Gemini microscope under high vacuum condition and a primary electron energy of 3 keV. NP areas on glass substrates were electrically connected to the sample holder by conductive carbon adhesion tape.

Atomic Force Microscopy. Membrane thicknesses and surface topography were measured by an atomic force microscope (AFM) Solver Next (NT-MDT) in semicontact mode under ambient conditions using polysilicon probes with a typical resonant frequency of ∼140 kHz (HA_NC, NT-MDT).

UV−Vis Spectroscopy. For UV−vis characterization (transmission spectra), Au and AgNPs were immobilized on standard microscopy glass slides by means of an unstructured PHM that was subsequently removed by the plasma treatment step. As light source, we used a deuterium-tungsten halogen lamp (DH-2000-BAL, Micropack GmbH). The spectra were recorded with a grating spectrometer (HR2000, Ocean Optics).

3. RESULTS AND DISCUSSION

3.1. General Procedure. The proposed route is schematically shown in Figure 1. PEG hydrogel film, serving as

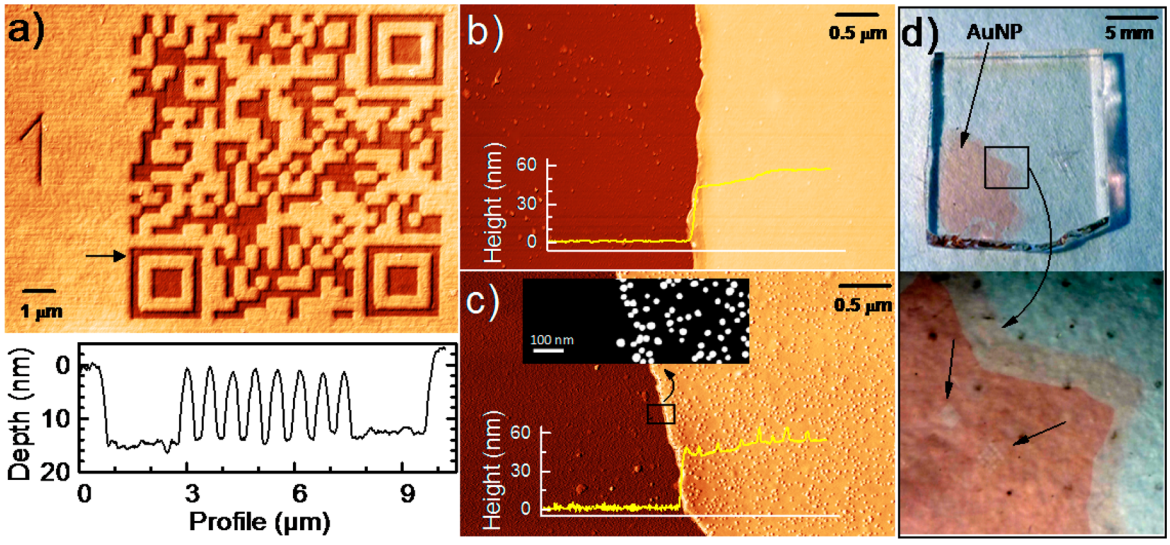

Figure 2. (a) AFM image of a glass supported PHM template with pattern of a QR code (29 by 29 modules) after transfer from the primary conductive support (top panel) as well as a height profile across one of the features as shown by the black arrow (bottom panel); (b) AFM image and height profile across the edge of the pristine PHM template; (c) the same records as in b collected after AuNP seeding (along with a corresponding SEM image in inset); (d) photographs of a glass slide after removal of the PHM template; the red color stems from AuNPs and emphasizes the margins of the original PHM template. The patterned areas are marked by black arrows.

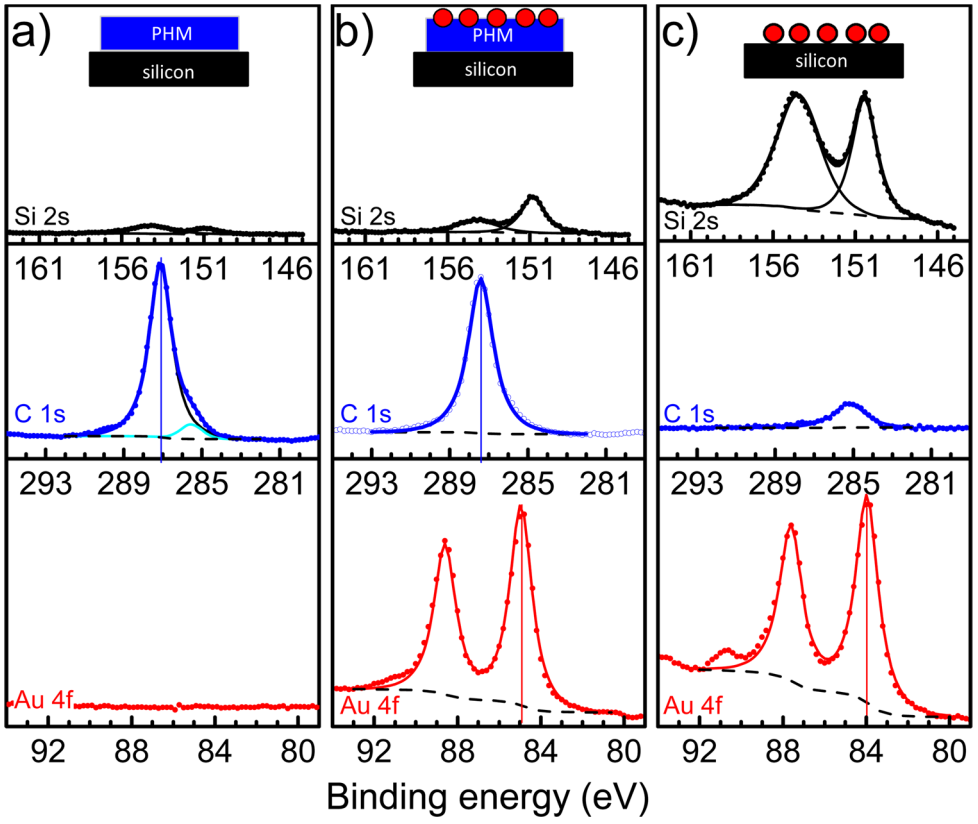

Figure 3. (a–c): Si 2s (top panels), C 1s (middle panels), and Au 4f (bottom panels) XP spectra acquired after the fundamental steps, viz. (a) transfer of pristine PHM onto a silicon substrate, (b) seeding of AuNPs into the PEG matrix, and (c) hydrogen plasma treatment.

precursor for the textured PEG hydrogel membrane, is initially prepared on a primary, conductive substrate of a polished silicon Si(100) wafer covered by a 100 nm gold layer. Typically, there is a 5 nm adhesion promoter between the Au film and the Si substrate. However, evaporating the Au film directly onto Si yields a weakly coupled Au film, which is, nevertheless, stable enough to survive the PHF preparation and patterning steps (schematically in Figure 1a). Dipping the wafer into water peels off the Au/PHF from the Si support (implied in Figure 1b), leaving the Au/PHF sheet on the surface of the water. The bilayer is transferred onto an aqueous gold etching solution where the sacrificial gold film is removed. The resulting patterned hydrogel template is subsequently transferred onto the secondary, target substrate (Figure 1c) and immersed into

dx.doi.org/10.1021/am504358a | ACS Appl. Mater. Interfaces 2014, 6, 14729–14735

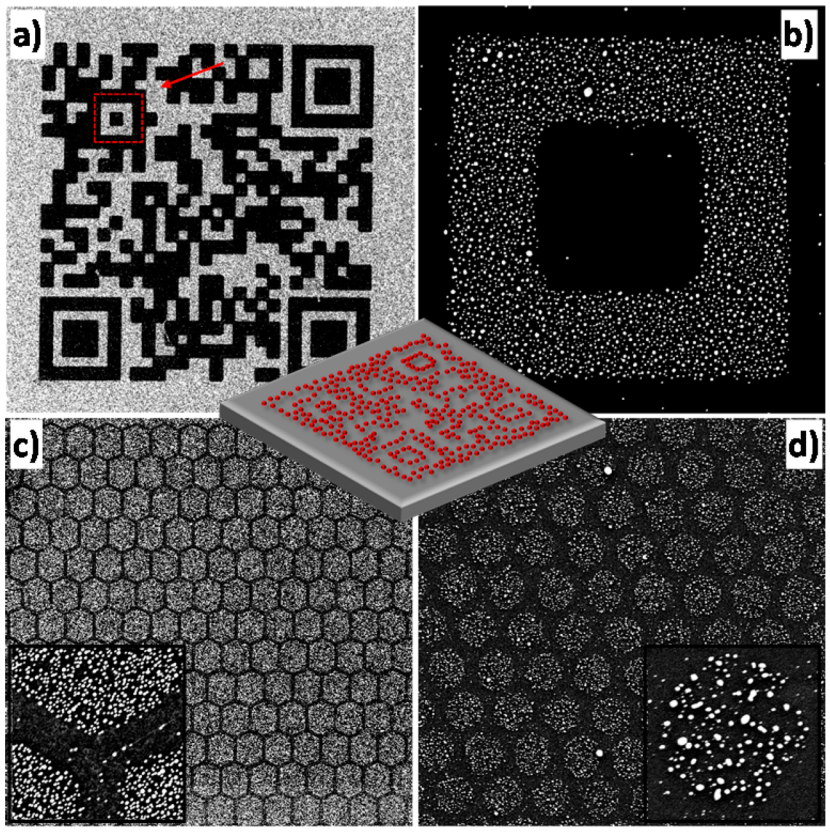

Figure 4. SEM images of NP patterns on glass acquired after removal of the PHM template: (a) AuNP pattern of a QR-code with 29 by 29 modules at a module size of 1 μm; the pattern is a perfect, negative reproduction of the original pattern written in the PHF by EBL (see Figure 2a); (b) high-resolution image of a single module marked by an arrow in a) makes individual NPs and high contrast clearly visible; (c) extract of large-area AuNP hexagon pattern (250 by 250 μm) with 300 nm separation between 3 μm hexagons; high density and contrast of NPs are demonstrated in the inset; (d) large-area AgNP circle (1 μm diameter; hexagonal arrangement) pattern; high density and contrast are well-visible in inset.

an aqueous solution of metal NPs followed by gently rinsing with water. NPs exclusively adsorb onto the nonirradiated areas of the PHM template (Figure 1d), mimicking its texture. Finally, the organic PHM matrix is completely removed by hydrogen plasma treatment, leaving the NP pattern as the only object on the substrate (Figure 1e). The latter step somewhat restricts potential NPs, as well as target substrates, to inorganic materials and inert polymers with high-temperature resistance, such as polytetrafluoroethylene.

Although the principles of EBL-assisted texturing of PEG hydrogel films (Figure 1a) have already been discussed,[35] it has to be demonstrated that the PHF patterns survive the lift-off/transfer process and are reproduced accurately in the PHM template relocated onto the secondary substrate (Figure 1c). Also it must be proven that the template is still directive to NP deposition as shown in Figure 1d.

As a test system, we used a PHF of 60 nm thickness and generated a pattern of a quick-response code (QR-code) consisting of 29 by 29 modules with an e-beam writer. This patterned PHF was removed from the primary substrate, the Au sacrificial layer dissolved, and the resulting PHM template placed onto a standard microscope glass slide as target substrate. The atomic force microscopy (AFM) image in Figure 2a clearly resolves the QR-code and shows no deviations from the original design. Regions exposed to electron beam appear ~17 nm deeper than the pristine background, corresponding to about one-third of the total membrane thickness (60 nm). This was estimated by recording a height profile across the membrane edge (Figure 2b). The QR-code in Figure 2a has a 300 nm module size and is, therefore, to our best knowledge, the smallest code ever reported. Particularly in combination with NPs, such miniaturized QR-codes can play a key role in fabricating μm-sized tamper-proof labels or "nanotaggants".[38,39]

Following the scheme in Figure 1, the PHM template was immersed into an aqueous solution of AuNPs with a diameter of ~35 nm. The thickness of the composite membrane did not change significantly after the seeding process, as shown in the corresponding height profile across the membrane edge (Figure 2c). Embedded AuNPs are clearly visible as bright spots in the AFM image, as well as narrow peaks in the height profile. No particles are detected on the uncovered glass surface, meaning that AuNPs do not adhere to the substrate background. This is further illustrated by a corresponding scanning electron microscopy (SEM) image of the template edge (inset in Figure 2c).

Finally, the PHM template with the embedded NPs was subjected to hydrogen plasma treatment, removing the organic matrix entirely and leaving the NPs as a firmly attached pattern on the glass slide. The area initially covered by the membrane can clearly be recognized in optical images (Figure 2d) by red color related to the LSPR excitation. No particles are detected on the uncovered glass surface.

3.2. XPS. To verify the efficiency of the procedure, we monitored AuNP seeding and plasma treatment steps by X-ray photoelectron spectroscopy (XPS) using doped silicon as

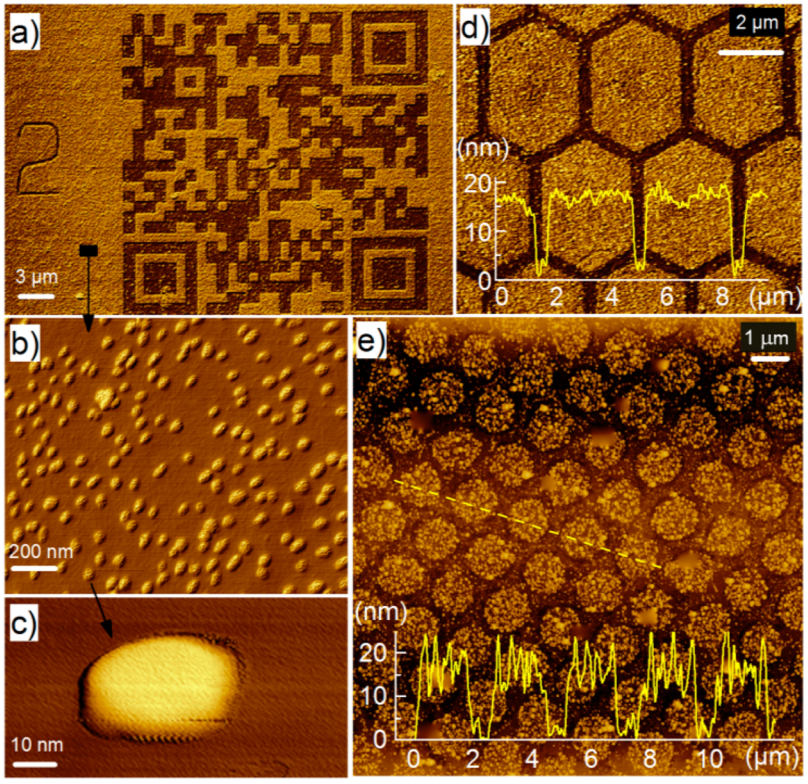

Figure 5. AFM images of (a–d) gold and (e)silver NP patterns on glass: (a) the QR-code from Figure 4a with a cell size of 1 μm; (b) high-resolution scan of the marked area and (c) image of an individual AuNP; (d) image of AuNP hexagon pattern presented in Figure 4c, along with the respective height profile; (e) image of AgNP circle pattern presented in Figure 4d as well as respective height profile along the yellow dashed line in the image.

secondary substrate to avoid charging effects. The spectra of pristine PHM in Figure 3a exhibit a strong carbon C 1s emission at ~287 eV typical of ether carbon of the PEG material. Due to the thickness of PHM, the Si 2p signal from the substrate is strongly attenuated and is hardly visible in the spectra. It remains weak after the deposition of AuNPs into PHM (Figure 3b), demonstrating the expected insolubility of the membrane in an aqueous solution (apart from weakly bound moieties). The carbon C 1s signal also suffers no significant changes apart from a minor decrease due to desorption of weakly bound fragments and attenuation by AuNPs. A weak emission at 285.2 eV is probably related to carbon contamination but disappears after AuNP adsorption. The strong Au 4f signal in Figure 3b, that was absent before (Figure 3a), is unambiguous evidence for the adsorption of AuNPs into the PEG matrix. The Au 4f doublet is slightly shifted (~1 eV) toward higher binding energies as compared to the standard position (84.0 eV for Au $4f_{7/2}$), which is a hint for a predominant location of NPs at the PEG-ambience interface. Plasma treatment successfully removes the PHM matrix. This is confirmed by an almost complete vanishing of the C 1s signal, accompanied by a significant increase of the Si 2s emission intensity(Figure 3c). At the same time, the intensity of the Au 4f signal remains nearly constant, while the doublet is shifted to 84.0 eV ($4f_{7/2}$), which is typical of metallic gold. The latter suggests a good electrical contact between AuNPs and substrate after removal of PHM. The persistence of the Au 4f intensity upon plasma treatment is a further indication that AuNPs are not randomly located in the PHF matrix but are predominantly deposited at PHF-ambience interface.

3.3. SEM. Scanning electron microscopy (SEM) usually requires conductive substrates such as doped silicon for distortion-free imaging. However, high resolution images of AuNP patterns could also be obtained on insulating glass slides when the NP containing area was connected to the sample holder by conductive adhesion tape. SEM images of the NP-covered areas in Figure 4 differ sharply from the pristine glass substrate and the QR-code formed by AuNPs in Figure 4a (1 μm module size) represents a perfect, negative reproduction of the original EBL pattern in the PHF (according to Figure 2a). The high contrast is obvious, with almost no particles identifiable in areas where the parent PHF template was exposed to the e-beam. The high resolution SEM image in Figure 4b emphasizes this superb contrast, as well as sharp boundaries and high packing density of the AuNPs (~400 NPs per μm^2 corresponding to a surface coverage of ~40% at a mean particle diameter of 35 nm). Even at high magnification, individual AuNPs are clearly resolved and no distortion due to charging effects, typical of insulating glass substrate, is perceptible. The density of the AuNPs is apparently sufficient to prevent effective charging of the sample.

An inverse, negative pattern of NPs compared to the primary EBL pattern is one of the benefits of our method. This is demonstrated in Figure 4c where comparably large AuNP hexagons (3 μm) arranged in a hexagonal pattern are separated by 300 nm thin, almost NP-free stripes. The borders of the hexagons are well-defined and it should be possible to achieve a resolution of 100 nm or higher, as was shown for PHFs on the primary substrates.[35]

The third advantage of our method arises from the ability of the PHM template to embed not only AuNPs but also other

inorganic NPs, which can be prepared or dissolved in water. In Figure 4d, for instance, silver NPs (AgNPs) are arranged on a glass substrate in a hexagonal pattern comprising NP containing circles with a diameter of 1 μm. Similar to AuNPs, Ag particles are deposited in high densities. However, they are characterized by a broader size distribution as shown in the inset of Figure 4d.

3.4. AFM. Complementary to SEM imaging, we also performed AFM characterization of fabricated NP patterns on a glass support. In contrast to SEM, AFM offers nondestructive, topographic images with nanometer resolution on nonconductive samples under ambient conditions. Figure 5a shows an AFM image of the AuNP pattern on glass presented in the SEM image in Figure 4a. The QR-code structure is clearly visible and individual NPs are distinguishable as shown in Figure 5b. The NP dimensions are well-reproduced but there is a deviation from the spherical form as seen in Figure 5c, which is likely to be due to tip convolution. Also, the large area AuNP and AgNP patterns presented in panels c and d in Figure 4, respectively, are well reproduced by AFM (Figures 5d and 5e). Higher NP density in case of Au as compared to Ag can be traced in the respective height profiles. Within NP covered areas, they show more or less constant signal for Au (Figure 5d) in contrast to the pronounced, NP related spikes for Ag (Figure 5e). However, both for Au and Ag, the stripes between NP covered areas are well-defined and exhibit very few (if any at all) NPs.

3.5. UV–Vis. As mentioned above, gold and silver NPs are particularly interesting due to their extraordinary optical properties, manifesting in an unusually strong absorption maximum close to SPR. As a representative example, Figure 6 presents the transmission UV–vis spectra of AuNPs (solid line) and AgNPs (dashed line) immobilized, with a help of a hydrogel membrane, on a glass slide, which exhibits no defined absorption features (dotted line). Although in both cases the surface density of NPs is lower than 0.5 monolayers (see Figures 3 and 4), the characteristic SPR bands are obvious. For AuNPs with a diameter of 35 nm, the resonance appears at ~530 nm whereas the excitation for silver NPs is blue-shifted to ~410 nm. Also, the absorption band of AgNPs is broader due to their larger size distribution compared to AuNPs. Note that AgNPs generally exhibit a stronger resonance than AuNPs, which is also confirmed in Figure 6, assuming similar grafting densities.

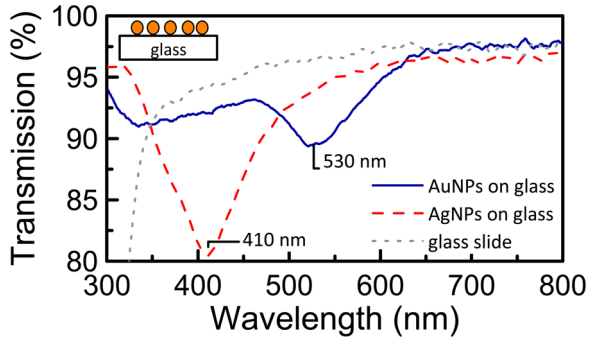

Figure 6. UV–vis transmission spectra of AuNPs (blue solid line) and AgNPs (red dashed line) immobilized on glass slides (particle density <0.5 monolayers) showing the characteristic SPR as a well-defined transmission minimum; for comparison, the corresponding spectrum of a pristine glass slide (black dotted line) without NPs.

4. CONCLUSION

We demonstrated a new approach to preparing custom-designed NP patterns on arbitrary substrates, including insulating ones. The approach relies on ultrathin hydrogel films (PHF) and related membranes (PHM) comprised of highly cross-linked, star-branched PEGs. The membranes are used as transient templates for laterally controlled deposition of inorganic NPs, mediated by the unique ability of the hydrogel matrix to adsorb such NPs directly from an aqueous solution. This adsorption ability can be quenched in a controlled fashion by electron irradiation, providing a unique template for the NP adsorption. This template is initially created on a primary conductive substrate, transferred to an arbitrary secondary substrate, and removed after NP adsorption, leaving the desired NP pattern. The efficiency of the approach was illustrated by creating a variety of tailor-made submicrometer patterns of gold and silver NPs on glass corresponding to a negative image of the areas treated by an electron beam. This allows significant reduction in exposure time for patterns where large areas covered with NPs are separated by thin, NP-free stripes. A further benefit of the approach is the possibility to prepare NP patterns not only on flat but also on curved or rough substrates.

AUTHOR INFORMATION

Corresponding Author

*E-mail: Michael.Zharnikov@urz.uni-heidelberg.de.

Present Address

[†]N.M. is currently at EaStCHEM School of Chemistry, University of St Andrews, North Haugh, St Andrews, KY16 9ST, UK.

Author Contributions

All authors contributed equally. The manuscript was written through contributions of all authors. All authors have given approval to the final version of the manuscript.

Funding

This work has been supported by the Volkswagen Stiftung (83227) and DFG (Ec 152/4–1).

Notes

The authors declare no competing financial interest.

ACKNOWLEDGMENTS

We thank Wolfgang Eck for initiation of this project, Michael Grunze for the support, and Hannah Aitchison for helping with the manuscript.

REFERENCES

(1) Parak, W. J.; Manna, L.; Simmel, F. C.; D, G.; P, A. Nanoparticles: From Theory to Application. In *Nanoparticles: From Theory to Application*, 2nd ed.; Schmid, G., Ed. Wiley–VCH: Weinheim, Germany, 2004.

(2) Daniel, M. C.; Astruc, D. Gold Nanoparticles: Assembly, Supramolecular Chemistry, Quantum-Size-Related Properties, and Applications Toward Biology, Catalysis, and Nanotechnology. *Chem. Rev.* **2004**, *104*, 293–346.

(3) Lee, K. S.; El-Sayed, M. A. Gold and Silver Nanoparticles in Sensing and Imaging: Sensitivity of Plasmon Response to Size, Shape, and Metal Composition. *J. Phys. Chem. B* **2006**, *110*, 19220–19225.

(4) Sardar, R.; Funston, A. M.; Mulvaney, P.; Murray, R. W. Gold Nanoparticles: Past, Present, and Future. *Langmuir* **2009**, *25*, 13840–13851.

(5) Raschke, G.; Kowarik, S.; Franzl, T.; Sonnichsen, C.; Klar, T. A.; Feldmann, J.; Nichtl, A.; Kurzinger, K. Biomolecular Recognition

Based on Single Gold Nanoparticle Light Scattering. *Nano Lett.* **2003**, *3*, 935−938.
(6) Zhao, J.; Zhang, X. Y.; Yonzon, C. R.; Haes, A. J.; Van Duyne, R. P. Localized Surface Plasmon Resonance Biosensors. *Nanomedicine* **2006**, *1*, 219−228.
(7) Kooyman, R. P. H. Physics of Surface Plasmon Resonance. In *Handbook of Surface Plasmon Resonance*, 1st ed.; Schasfoort, R. B. M., Tudos, A. J., Eds. RSC Publishing: Cambridge, U.K., 2008; Vol. *1*, pp 15−33.
(8) Saha, K.; Agasti, S.; S. Kim, C.; Li, X.; Rotello, V. M. Gold Nanoparticles in Chemical and Biological Sensing. *Chem. Rev.* **2012**, *112*, 2739−2779.
(9) Willets, K. A.; Van Duyne, R. P. Localized Surface Plasmon Resonance Spectroscopy and Sensing. *Annu. Rev. Phys. Chem.* **2007**, *58*, 267−297.
(10) Kim, Y. N.; Yoo, S. H.; Cho, S. O. Fabrication of SERS-Active Patterned Gold Nanoparticle Films by Electron Irradiation and Postpyrolysis. *J. Phys. Chem. C* **2009**, *113*, 618−623.
(11) Eck, W.; Craig, G.; Sigdel, A.; Ritter, G.; Old, L. J.; Tang, L.; Brennan, M. F.; Allen, P. J.; Mason, M. D. PEGylated Gold Nanoparticles Conjugated to Monoclonal F19 Antibodies as Targeted Labeling Agents for Human Pancreatic Carcinoma Tissue. *ACS Nano* **2008**, *2*, 2263−2272.
(12) Ofir, Y.; Samanta, B.; Rotello, V. M. Polymer and Biopolymer Mediated Self-Assembly of Gold Nanoparticles. *Chem. Soc. Rev.* **2008**, *37*, 1814−1823.
(13) Murray, R. W. Nanoelectrochemistry: Metal Nanoparticles, Nanoelectrodes, and Nanopores. *Chem. Rev.* **2008**, *108*, 2688−2720.
(14) Shipway, A. N.; Katz, E.; Willner, I. Nanoparticle Arrays on Surfaces for Electronic, Optical, and Sensor Applications. *ChemPhysChem* **2000**, *1*, 18−52.
(15) Liao, J. H.; Li, X. X.; Wang, Y.; Zhang, C. Y.; Sun, J. L.; Duan, C.; Chen, Q.; Peng, L. M. Patterned Close-Packed Nanoparticle Arrays with Controllable Dimensions and Precise Locations. *Small* **2012**, *8*, 991−996.
(16) Sato, T.; Ahmed, H.; Brown, D.; Johnson, B. F. G. Single Electron Transistor Using a Molecularly Linked Gold Colloidal Particle Chain. *J. Appl. Phys.* **1997**, *82*, 696−701.
(17) Liu, X. G.; Fu, L.; Hong, S. H.; Dravid, V. P.; Mirkin, C. A. Arrays of Magnetic Nanoparticles Patterned via "Dip-Pen" Nanolithography. *Adv. Mater.* **2002**, *14*, 231−234.
(18) Anker, J. N.; Hall, W. P.; Lyandres, O.; Shah, N. C.; Zhao, J.; Van Duyne, R. P. Biosensing with Plasmonic Nanosensors. *Nat. Mater.* **2008**, *7*, 442−453.
(19) Aydin, D.; Schwieder, M.; Louban, I.; Knoppe, S.; Ulmer, J.; Haas, T. L.; Walczak, H.; Spatz, J. P. Micro-Nanostructured Protein Arrays: A Tool for Geometrically Controlled Ligand Presentation. *Small* **2009**, *5*, 1014−1018.
(20) Glass, R.; Arnold, M.; Cavalcanti-Adam, E. A.; Blummel, J.; Haferkemper, C.; Dodd, C.; Spatz, J. P. Block Copolymer Micelle Nanolithography on Non-Conductive Substrates. *New J. Phys.* **2004**, *6*, 101.
(21) Santhanam, V.; Andres, R. P. Microcontact Printing of Uniform Nanoparticle Arrays. *Nano Lett.* **2004**, *4*, 41−44.
(22) Yang, Ki-Y.; Kim, J.-W.; Byeon, K.-J.; Lee, H. Selective Deposition of the Silver Nano-particles Using Patterned the Hydrophobic Self-Assembled Monolayer Patterns and Zero-Residual Nano-Imprint Lithography. *Microelectron. Eng.* **2007**, *84*, 1552−1555.
(23) Barbillon, G.; Hamouda, F.; Held, S.; Gogol, P.; Bartenlian, B. Gold Nanoparticles by Soft UV Nanoimprint Lithography Coupled to a Lift-off Process for Plasmonic Sensing of Antibodies. *Microelectron. Eng.* **2010**, *87*, 1001−1004.
(24) Wang, W. M.; Stoltenberg, R. M.; Liu, S.; Bao, Z. Direct Patterning of Gold Nanoparticles Using Dip-Pen Nanolithography. *ACS Nano* **2008**, *2*, 2135−2142.
(25) Fresco, Z. M.; Frechet, J. M. J. Selective Surface Activation of a Functional Monolayer for the Fabrication of Nanometer Scale Thiol Patterns and Directed Self-Assembly of Gold Nanoparticles. *J. Am. Chem. Soc.* **2005**, *127*, 8302−8303.
(26) Corbierre, M. K.; Beerens, J.; Lennox, R. B. Gold Nanoparticles Generated by Electron Beam Lithography of Gold(I)-Thiolate Thin Films. *Chem. Mater.* **2005**, *17*, 5774−5779.
(27) Glass, R.; Möller, M.; Spatz, J. P. Block Copolymer Micelle Nanolithography. *Nanotechnology* **2003**, *14*, 1153−1160.
(28) Lohmüller, T.; Aydin, D.; Schwieder, M.; Morhard, C.; Louban, I.; Pacholski, C.; Spatz, J. P. Nanopatterning by Block Copolymer Micelle Nanolithography and Bioinspired Applications. *Biointerphases* **2011**, *6*, Mr1−Mr12.
(29) Mendes, P. M.; Jacke, S.; Critchley, K.; Plaza, J.; Chen, Y.; Nikitin, K.; Palmer, R. E.; Preece, J. A.; Evans, S. D.; Fitzmaurice, D. Gold Nanoparticle Patterning of Silicon Wafers Using Chemical e-Beam Lithography. *Langmuir* **2004**, *20*, 3766−3768.
(30) Zhao, J. L.; Terfort, A.; Zharnikov, M. Gold Nanoparticle Patterning on Monomolecular Chemical Templates Fabricated by Irradiation-Promoted Exchange Reaction. *J. Phys. Chem. C* **2011**, *115*, 14058−14066.
(31) Werts, M. H. V.; Lambert, M.; Bourgoin, J. P.; Brust, M. Nanometer Scale Patterning of Langmuir-Blodgett Films of Gold Nanoparticles by Electron Beam Lithography. *Nano Lett.* **2002**, *2*, 43−47.
(32) Hamann, H. F.; Woods, S. I.; Sun, S. H. Direct Thermal Patterning of Self-Assembled Nanoparticles. *Nano Lett.* **2003**, *3*, 1643−1645.
(33) Prinz, G. A. Device physics - Magnetoelectronics. *Science* **1998**, *282*, 1660−1663.
(34) Meyerbröker, N.; Kriesche, T.; Zharnikov, M. Novel Ultrathin Poly(ethylene glycol) Films as Flexible Platform for Biological Applications and Plasmonics. *ACS Appl. Mater. Interfaces* **2013**, *5*, 2641−2649.
(35) Meyerbröker, N.; Zharnikov, M. Modification and Patterning of Nanometer-Thin Poly(ethylene glycol) Films by Electron Irradiation. *ACS Appl. Mater. Interfaces* **2013**, *5*, 5129−5138.
(36) Meyerbröker, N.; Zharnikov, M. Ultraflexible, Freestanding Nanomembranes Based on Poly(ethylene glycol). *Adv. Mater.* **2014**, *26*, 3328−3332.
(37) Lee, P. C.; Meisel, D. Adsorption and Surface-Enhanced Raman of Dyes on Silver and Gold Sols. *J. Phys. Chem.* **1982**, *86*, 3391−3395.
(38) Han, S.; Bae, H. J.; Kim, J.; Shin, S.; Choi, S. E.; Lee, S. H.; Kwon, S.; Park, W. Lithographically Encoded Polymer Microtaggant Using High-Capacity and Error-Correctable QR Code for Anti-Counterfeiting of Drugs. *Adv. Mater.* **2012**, *24*, 5924−5929.
(39) Sangeetha, N. M.; Moutet, P.; Lagarde, D.; Sallen, G.; Urbaszek, B.; Marie, X.; Viau, G.; Ressier, L. 3D Assembly of Upconverting NaYF4 Nanocrystals by AFM Nanoxerography: Creation of Anti-Counterfeiting Microtags. *Nanoscale* **2013**, *5*, 9587−9592.